Journal Pre-proof

Regio-isomerism Directed Electrocatalysis for Energy Efficient Zinc-air Battery

Sanchayita Mukhopadhyay, Mruthyunjayachari Chattanahalli Devendrachari, Sandeep C. Kanade, Chathakudath Prabhakaran Vinod, Harish Makri Nimbegondi Kotresh, Musthafa Ottakam Thotiyl

PII: S2589-0042(22)01451-1

DOI: https://doi.org/10.1016/j.isci.2022.105179

Reference: ISCI 105179

To appear in: *ISCIENCE*

Received Date: 15 July 2022

Revised Date: 29 August 2022

Accepted Date: 19 September 2022

Please cite this article as: Mukhopadhyay, S., Devendrachari, M.C., Kanade, S.C, Vinod, C.P., Nimbegondi Kotresh, H.M., Thotiyl, M.O., Regio-isomerism Directed Electrocatalysis for Energy Efficient Zinc-air Battery, *ISCIENCE* (2022), doi: https://doi.org/10.1016/j.isci.2022.105179.

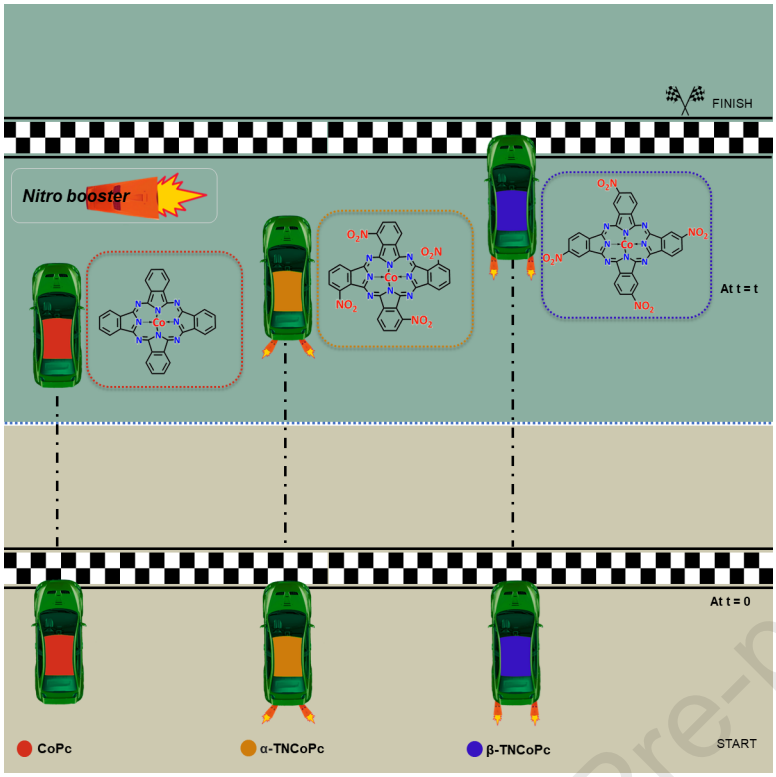

Article

Regio-isomerism Directed Electrocatalysis for Energy Efficient Zinc-air Battery

Sanchayita Mukhopadhyay,[1] Mruthyunjayachari Chattanahalli Devendrachari,[1] Sandeep C Kanade,[1] Chathakudath Prabhakaran Vinod,[2] Harish Makri Nimbegondi Kotresh,[3] and Musthafa Ottakam Thotiyl [1,4,*]

[1]Department of Chemistry and Centre for Energy Science, Indian Institute of Science Education and Research, Pune, Dr. Homi Bhabha Road, Pune 411008, India.

[2]Catalysis and Inorganic Chemistry Division, CSIR-NCL, Pune 411008, India.

[3]Department of Chemistry, Acharya Institute of Technology, Soldevanahalli, Bangalore 560107, India.

[4]Lead contact

*Correspondence: musthafa@iiserpune.ac.in

SUMMARY

We have investigated the role of ligand-isomerism in modulating the mechanisms and kinetics associated with charge/discharge-chemistry of an aqueous metal-air battery. The dominant electron-withdrawing inductive effect (-I effect) and the diminished electron-withdrawing resonance effect (-R effect) in the α-NO_2 isomer noticeably diminishes the rate of oxygen reduction (ORR) and oxygen evolution reactions (OER) on the catalytic Co-centre. In their β-counterpart, the cumulative –I and –R effects noticeably enhance the OER and ORR kinetics on the same catalytic Co-centre. Therefore, the regioisomerism of the -NO_2 functionality amplifies the kinetics of ORR/OER without influencing their mechanistic pathways. When isomeric electrocatalysts are integrated to aid the charge-chemistry of a Zn-air battery, the overpotential could be decreased by ~250 mV with β-NO_2 isomer leading to a round-trip efficiency as high as 60%. This work contributes to the design of novel molecular platforms to target the overall round-trip efficiency of energy storage and conversion devices.

INTRODUCTION

The ever-increasing demands for energy and awareness about climate change have made the transition from a fossil fuel-based energy economy to an alternative clean energy economy inevitable(Davidson, 2019)(Gao et al., 2021)(Ledendecker et al., 2015). This gradual process has been accelerated by recent research worldwide on sustainable energy harvesting, conversion and storage(Chinnam et al., 2015)(Indra et al., 2018)(Liberman et al., 2020). In this context, various types of batteries have been developed with myriads of applications ranging from portable electronic devices, grid-scale energy storage to electric vehicles(Zhao et al., 2022)(Harper et al., 2019)(W. Li et al., 2019)(Zhang et al., 2022)(Tabassum et al., 2019). Among these, metal-air battery technologies such as Zn-air batteries (ZABs) are projected as promising candidates for long driving range electric vehicles (EVs) mainly because of their high gravimetric energy densities in the range of 470 W h kg^{-1}(Bruce et al., 2012)(Lee et al., 2011)(Jung et al., 2016)(Li et al., 2021). However, there are several challenges associated with aqueous rechargeable metal–air batteries. Firstly, it suffers from high charge/discharge overpotential due to the high overvoltage for oxygen evolution reaction (OER) and oxygen reduction reaction (ORR) which consequently leads to low round trip efficiency typically in the range of ~50-60 %(Liu et al., 2019)(Guo et al., 2018)(Liu et al., 2016). As far as ORR is concerned, the reaction is catalyzed by benchmark Pt based noble metal electrocatalysts, which has several issues associated with cost and availability(Fu et al., 2017)(Peng et al., 2022). This necessitates exploration of durable electrocatalysts based on earth abundant non-noble metals. Secondly, ORR can proceed through variety of pathways and hence catalysts catalyzing the 4 electron ORR is often preferred for aqueous air-batteries(Özen et al., 2016)(Xu et al., 2019). Besides, the higher charge voltage associated with OER often results in

the degradation or corrosion of the air electrode, thereby, greatly reducing the cycle life of aqueous air batteries(Li et al., 2022)(Lee et al., 2014). Moreover, the benchmark OER electrocatalysts like IrO_2, RuO_2 etc., are low in abundance and consequently have high cost and are not very stable in strongly alkaline electrolytes which is often encountered in aqueous metal air batteries(Cherevko et al., 2016)(Ghareghashi and Mohebbi, 2020). In this context, the need of the hour is to develop alternative oxygen reduction reaction (ORR) / oxygen evolution reaction (OER) catalysts based on earth-abundant metals with high activity and durability for rechargeable ZABs(Özen et al., 2016)(Xu et al., 2019)(Bhowmick et al., 2020)(Anju et al., 2016).

Herein, we aim to explore ligand isomerism in molecular electrocatalysts like phthalocyanines for the ZAB discharge/charge reaction (ORR/OER) to target their overall round-trip efficiency. The choice of phthalocyanines is mainly based on the fact that these molecules are among the prime candidates that are being explored for various electrochemical applications because of their robustness, stability and highly tuneable optoelectronic properties(Sobbi et al., 1993)(Bottari et al., 2010)(Complexes, 2007)(Sorokin, 2013). Among these phthalocyanines, we have explored the Co based systems as they have been found to be electrocatalytically active towards ORR/OER(Kottaichamy et al., 2020)(Cong et al., 2005)(Fu et al., 2020)(C. Li et al., 2019). Interestingly, when nitro substituted cobalt phthalocyanines (TNCoPc) were explored for ZAB discharge/charge reaction, we found that the ligand isomerism (α and β-TNCoPc isomers) significantly tunes their respective kinetics without altering the mechanistic pathways of the reaction. The present work demonstrates an alternative approach in the design of efficient molecular electrocatalysts to target electrochemical reactions relevant to energy storage and conversion.

RESULTS

Synthesis and characterization of isomeric molecules

In our previous work, we have shown that isomerism of $-NO_2$ functionality leads to an oxidative activation of catalytic metal centre which in turn aids oxidative electrocatalysis. However, whether the isomerism of the functionality influences the reaction mechanism or reaction kinetics with respect to a specific reaction pathway is still uncertain. To shed light into these issues, we have explored nitro substituted phthalocyanines containing earth abundant central metals like Co to target oxygen reduction (ORR) and oxygen evolution (OER) reactions. This is because, the complexity of ORR/OER is the limiting factor which dictates the round-trip efficiency of aqueous metal-air batteries and reversible fuel cells(Liu et al., 2019)(Guo et al., 2018)(Liu et al., 2016). To explore the implications of ligand isomerism in ORR/OER; we have synthesized and characterized the regioisomers of tetra-nitro cobalt phthalocyanine (TNCoPc) with $-NO_2$ substitution at the α (α-TNCoPc) and β (β-TNCoPc) positions, Scheme 1 as reported previously(Sobbi et al., 1993)(Bottari et al., 2010)(Complexes, 2007)(Sorokin, 2013)(Kottaichamy et al., 2020)(Cong et al., 2005)(Fu et al., 2020)(C. Li et al., 2019). High-resolution mass spectrometry (HRMS) demonstrated the parent ion peak at m/z value of ~751 for the α and β isomers and at ~573 for unsubstituted cobalt phthalocyanine (CoPc) which are close to their molecular masses, (Figure S1a, b and c). UV-vis, FTIR and Raman spectroscopy further demonstrate the formation of isomeric molecules in line with the literature (Figure S2a, b, c, Table S1 and Table S2) (Kottaichamy et al., 2020)(Cong et al., 2005)(Li et al., 2006)(Kobayashi et al., 2002)(Panwar et al., 2015)(Topuz et al., 2013)(Zhu et al., 2014)(Georgescu et al., 2015). 1D and 2D NMR spectroscopic analysis further confirm the formation of isomeric molecules, (Figure S2d, e and f) (Kottaichamy et al., 2020).

The primary aim of this investigation is to understand how the isomerism of the $-NO_2$ functionality influences the reaction mechanism /reaction kinetics of ORR/OER so as to explore their potential to improve the overall energy efficiency of a Zn air battery. Toward this, isomeric molecular catalysts were first anchored on carbon nanotubes (CNT) because of its known capability to aid electron transport(Zhang and Gorski, 2005)(Abbaspour and Mirahmadi, 2013)(Chidembo et al., 2010)(Zhu et al., 2011)(Zhang et al., 2017). α and β-TNCoPcs and unsubstituted CoPc anchored on CNT (α-TNCoPc/CNT, β-TNCoPc/CNT and CoPc/CNT) were synthesized(Kottaichamy et al., 2020) and characterized by FTIR, Raman spectroscopy, UV-visible spectroscopy along with Scanning electron microscopy (SEM) and energy dispersive X-ray spectroscopy (EDS) techniques, (Figure S3, Figure S4, Figure S5 and

Table S3). The features of CNT in the TNCoPc/CNT catalytic system in the FTIR, Raman spectra and SEM images suggest the formation of CNT composite catalytic systems, (Figure S3a, and Figure S3b) as provided in Supplemental Information. The EDS data (Figure S5 and Table S3) confirm the amount of Co present in all the three composite catalytic system is maintained more or less the same.

Kinetic and mechanistic investigations of ORR/OER

Linear sweep voltammograms (Figure 1a), suggest that the activity of β-TNCoPc isomer towards the half-cell ORR/OER is superior to its α counterpart which is clear from the onset potential and potential required for achieving a particular rate (Table S4), (refer to experimental section for details). Since the catalytic domain is the central metal ion (cobalt ion), voltametric investigation reveals that ligand isomerism can tune the catalytic metal center with the 'β' isomer demonstrating enhanced ORR/OER activities compared to the corresponding 'α' isomer, (Figure 1a). This will be beneficial for improving the round-trip efficiency in metal-air batteries as ORR/OER is their discharge/charge reactions respectively(Li et al., 2022)(Lee et al., 2014)(Cherevko et al., 2016)(Ghareghashi and Mohebbi, 2020). Hydrodynamic voltammetry for ORR shows that, the number of electron transferred is close to 3 and % of peroxide is close to 50 % for both the isomeric molecules, suggesting that ORR proceeds with the intermediacy of peroxide, (Figure 1b). The Tafel analysis (Figure 1c and Figure S6) suggest a lower Tafel slope for the β isomer indicating a facile kinetics in this isomer. The long-term stability is then subsequently investigated on isomeric electrocatalysts in the half-cell modes by chronopotentiometric analysis. Clearly, the potential required to achieve the same current density is substantially lower in β-isomer compared to α-isomer, (Figure 1d). This indicate that isomerism of -NO_2 functionality does not change the ORR reaction mechanism. However, it does change the kinetics of ORR substantially, with a higher activity in favour of the β-isomer compared to the α-isomer, (Figure 1). Secondly, this pathway with the intermediacy of peroxide is desirable for the electrosynthesis of peroxide but detrimental for energy conversion devices, as peroxide is known to poison the electrocatalytic domains.

Though water oxidation is superior in β-isomer over the corresponding α-isomer (Figure 1a and Figure S7), it is known that water oxidation can lead to the formation of peroxide ($2e^-$ pathway) or O_2 ($4e^-$ pathway, OER) as the products(Shi et al., 2021)(Xia et al., 2020)(Gill et al., 2021). The former is desirable for peroxide electrosynthesis but the latter for energy conversion devices(Malali et al., 2020)(Zhang et al., 2020)(Wu et al., 2020). To prove this unambiguously, rotating ring disk electrode (RRDE) measurements were carried out by performing linear sweep voltammetry at the disk for OER and biasing the ring (Au ring) at ORR potential (0.7 V vs. RHE) and peroxide oxidation potential (1 V vs. RHE), (Figure 2a). The corresponding potentials were determined from the cyclic voltammogram, (Figure S8) for oxygen reduction reaction and peroxide oxidation on Au electrodes. When the ring is biased at ORR potentials (0.7 V vs. RHE), the ring current appears as soon as the disk potentials cross the water oxidation regime. However, no ring current is seen when it is biased at peroxide oxidation potential, (Figure 2a). This clearly suggests O_2 is the primary product during water oxidation at the disk and not the peroxide. The Tafel plot, (Figure 2b), shows a facile kinetics on the β-isomer compared to α-isomer and unsubstituted CoPc. The long-term stability with a higher activity is observed on the β-isomer compared to the α-isomer, (Figure 2c). All these indicate that, the isomerism of the -NO_2 functionality does not change the reaction mechanism of OER, however, it rather influences the reaction kinetics. Taken together, the ligand isomerism via the isomerism of -NO_2 functionality in the secondary sphere does not change the reaction dynamics of OER/ORR but it significantly influences their respective electrochemical kinetics. The data outlined in (Figure 1 and Figure 2) further demonstrate that ligand isomerism via the regio-isomerism of -NO_2 functionality can be utilized for aiding the charge reaction of an aqueous metal air battery and not the discharge chemistry due to the involvement of peroxide intermediacy in the latter.

The reason for this fascinating behaviour with respect to regioisomerism can be primarily attributed to the electron withdrawing resonance effect (-R) and electron withdrawing inductive effect (-I) of the nitro groups (-NO_2) in the isomeric molecules(Kottaichamy et al., 2020)(Cong et al., 2005). The closeness of 'O' of –NO_2 group and the iminic 'N' atom in the macrocyclic ring of the α-isomer may prompt repulsive field effects between these groups which may force the –NO_2 group to go out of the molecular plane. This might lead to a reduction in the –R effect between –NO_2 group and the macrocycle plane and the electron

withdrawing effect may mainly originate from the -I effect. Whereas, for the β isomer, repulsive filed effect between the groups can be negligible as they are well separated spatially. This might favour an in-plane confirmation of $-NO_2$ group in β isomer leading to a dominant –R and –I effect in the molecule. This is in fact responsible for the broadening and red shifting of Q band in the β-TNCoPc isomer with respect to the Q band of α-TNCoPc isomer molecule (Figure S2a). Nevertheless, due to these circumstances the central metal ion should be more electron deficient in the β-isomer compared to the α-isomer. This should enhance the contribution of the oxidized Co species in the β-isomeric molecule compared to the α-isomeric molecule. This is reflected in the X- ray photoelectron spectroscopy (XPS) data of these molecules, (Figure 2d) wherein the binding energy peak corresponding to Co^{3+} ($2p_{3/2}$) species demonstrated a positive binding energy shift of 0.6 eV in the β-isomeric molecule compared to the α-isomeric molecule. These suggest that the contribution of oxidized cobalt species is noticeably enriched in the β-isomer molecule compared to the corresponding α counterpart, (Figure 2d), which in turn indicates a positive shift in the redox energy of Co^{3+}/Co^{2+} in the former(C. Li et al., 2019)(Gu et al., 2016)(Phys et al., 2019)(Thapa et al., 2021). This should lead to a better overlap of Co^{3+}/Co^{2+} redox energy level with the oxygen redox level in the β-isomer molecule which can amplify the oxygen redox reactions. This will be beneficial to boost the round-trip efficiency of ZABs as demonstrated below.

Evaluation of Zinc-air battery performance

In order to validate the performance of isomeric catalysts in Zn air battery, these molecules anchored on CNT were utilized as the OER catalysts during the charge chemistry in tri-electrode ZAB configuration as shown in (Scheme S1)(Cao et al., 2013)(Tran et al., 2020)(Hong et al., 2016). The discharge chemistry was carried out between Zn electrode and a Pt/C based ORR catalyst and the charge chemistry was carried out between the Zn electrode and the isomeric catalysts. The Zn half-cell and ORR/OER half-cells were separated by a Nafion 117 membrane. The discharge polarization curve demonstrated a peak power density of 90 mW/cm^2 at a current density of 150 mA/cm^2 (Figure S9), which is in line with the literature with Pt based catalysts(Yu et al., 2016)(Yu et al., 2016). The charge polarization curves show that the β-isomer outperforms the corresponding α-isomer and the charging reaction at all current densities occurs at a lower operating potential in the β-isomer than the α-isomer, (Figure 3a). The long-term stability was investigated by chronopotentiometry at a current density of 20 mA/cm^2 and it further show a lower operating potential in β-isomer than the corresponding α-isomer, (Figure 3b). In order to investigate the stability of metal air battery during repeated charge discharge, cyclic stability of the battery was investigated at a discharge and charge current density of 20 mA/cm^2, (Figure 3c), which further demonstrates that β-isomer requires a lower driving force than the corresponding α-isomer for achieving the same rate. Therefore, the round-trip efficiency is noticeably improved in the β-isomer compared to the α-isomer, (Figure 3d). In-situ electrochemical mass spectrometric data with the best performing β-isomer OER catalyst, show that when the cell is ON, the catalyst evolves oxygen and the oxygen signal decays to the base line when the cell is OFF, and the process is sustainable for several cycles, (Figure 3e). Further, we have carried out the cycling stability test of ZAB with the β isomer and it shows a stable charging profile for large number of cycles (70 cycles are shown), (Figure 3f). All these studies clearly suggest the β-isomer is an efficient material for improving the round-trip efficiency of rechargeable zinc air batteries. Further, we have made a comparison of the performance of our Zn-air battery employing the β-isomer with the Zn-air batteries reported in the literature (Table S5), which show the charging voltage and round-trip efficiency are comparable to the literature.

In order to investigate the durability of the β-isomer catalyst, post electrochemical characterization were carried after cycling the battery for 70 hours. X-ray photoelectron spectroscopy studies show that the Co signals are intact in the molecule before and after the long-term analysis and no signals of cobalt oxides were observed, (Figure 4a). UV-visible, FTIR and Raman spectroscopy reveal that the chemical identity of the molecular catalysts is well preserved even after prolonged electrocatalysis. These spectroscopic characterizations also rule out the possibility of CoOx formation by the degradation of the molecular catalysts. If it would have been formed, FTIR and Raman spectra would have shown characteristics peaks of CoOx which were not observed in the present case (Figure 4c and Figure 4d)(Li et al., 2016)(Tang et al., 2008)(Barakat et al., 2008). Taken together, we have demonstrated that ligand isomerism can be utilized to design non-precious molecular electrocatalysts for targeting the round trip efficiency of ZABs. This demonstration is expected to contribute to

the design of future molecular catalysts with improved activities for various electrochemical applications.

DISCUSSION

We have demonstrated the role of ligand isomerism in -NO_2 substituted molecular catalysts in tuning the reaction kinetics and reaction mechanisms of half-cell ORR and OER reactions. Oxidative activation in the β-isomeric electrocatalyst due to the combined presence of –R and –I effects as compared to the only –I effect in the α-isomeric electrocatalyst noticeably enhance the ORR and OER kinetics in the former, however, without altering their respective reaction mechanism. With respect to ORR on isomeric electrocatalysts, the number of electrons transferred were close to 3 and the percentage of peroxide was close to 50% on both the electrocatalysts, yet with an improved kinetics in the β-isomer. As far as OER is concerned, a 4 electron pathway was always preferred on both the isomeric electrocatalysts, however with a noticeably higher activity in favor of the β-isomer. To show the practical applicability in metal- air batteries, we have further shown how the the isomeric electrocatalysts influence the round-trip efficiency of Zn-air batteries by tuning the electrochemical kinetics associated with the OER charge chemistry. The results show that the β-isomer outperforms the α-isomer in terms of charging voltage and round-trip efficiency with excellent cycling stability. Nevertheless, the isomerism of -NO_2 functionality does not aid the discharge chemistry of Zn-air batteries because of the intermediacy of peroxide in the ORR pathway. However, this can be utilized as an electrocatalyst in peroxide electrosynthesising metal-air batteries and fuel cells(Shi et al., 2021)(Xia et al., 2020)(Gill et al., 2021)(Malali et al., 2020)(Brillas et al., 2002)(Li et al., 2013)(Li et al., 2013).

Limitations of the study

Overall, the work outlined shows a novel strategy towards the design of efficient molecular electrocatalysts to target the overall energy efficiency of future generation energy storage and conversion devices. We note that in the present work, the effect of isomerism of secondary sphere substituents on the charging chemistry is only demonstrated. In the future, the focus will be towards the development of bifunctional electrocatalysts based on earth abundant metal based phthalocyanines to aid the discharge as well as charge reactions. This is expected to help in the development of precious metal free air batteries.

ACKNOWLEDGMENTS

MOT is indebted to DST-SERB (CRG/2020/002549) and DST-WTI (DST/TMD-EWO/WTI/2K19/EWFH/2019/272) for financial support. S.M. thanks IISER Pune for financial support. Alagar Raja Kottaichamy and Zahid Manzoor Bhat are thanked for their initial assistance concerning characterization of isomeric molecules and air battery fabrications.

AUTHOR CONTRIBUTIONS

S.M. performed characterization of the molecules, electrochemical experiments, and battery performance measurements. M.C.D and H.M.N.K synthesized the molecules. S.C.K and C.P.V helped with the XPS analysis. M.O.T. supervised the work and wrote the manuscript. All the authors contributed to data analysis.

DECLARATION OF INTERESTS

The authors declare no competing interests.

Main figure titles and legends:

Scheme 1. Structures of ligand isomerism directed electrocatalysts.
Unsubstituted CoPc (Left), and isomeric α-TNCoPc (middle) and β-TNCoPc (right) molecules.

Figure 1. Mechanistic investigation of ORR on isomeric electrocatalysts.

(A) Linear sweep voltammograms for ORR as well as OER on α-TNCoPc and β-TNCoPc isomeric molecules.
(B) Plot showing the number of electrons and % of H_2O_2 formed with α-TNCoPc and β-TNCoPc isomeric molecules at a potential of 0.79 V vs. RHE.
(C) Tafel slopes for ORR with α-TNCoPc and β-TNCoPc isomers.
(D) Chronopotentiometric measurements for ORR at a constant current density of 0.5 mA/cm^2 for α-TNCoPc isomer and β-TNCoPc isomeric molecules.

Figure 2. Mechanistic investigation of OER on isomeric electrocatalysts.

(A) RRDE measurements during OER at the disk (red trace and violet trace) using α and β-TNCoPc isomeric molecules by biasing the Au ring at 0.7 V vs. RHE (pink and green trace) for ORR and at 1 V vs. RHE (orange and blue trace) for peroxide oxidation at 1600 RPM.
(B) Tafel plots along with their Tafel slopes for OER with unsubstituted CoPc, α-TNCoPc and β-TNCoPc isomers.
(C) Chronopotentiometric measurements at a constant current density of 10 mA/cm^2 for oxygen evolution reaction in pH=14 electrolyte at a rotation rate of 1600 RPM for unsubstituted CoPc, α-TNCoPc isomer and β-TNCoPc isomer.
(D) XPS spectra of pristine CoPc, α-TNCoPc and β-TNCoPc isomeric molecules.

Figure 3. Performance of a Zn-air battery charging chemistry with isomeric electrocatalysts.

(A) Charge-discharge profiles of rechargeable zinc–air batteries, discharge (black) and charge (blue, red, green) polarization curves obtained with Pt/C (0.5 mg/cm^2) as the ORR catalyst and β-TNCoPc, α-TNCoPc and unsubstituted CoPc as the OER catalysts (2 mg/cm^2) respectively.
(B) Chronopotentiometric traces at a constant current density of 20 mA/cm^2.
(C) Charge-discharge cycling data for ZAB with the isomeric molecular electrocatalysts at a current density of 20 mA/cm^2.
(D) Comparison of the round-trip efficiency at a current density of 20 mA/cm^2 for unsubstituted CoPc, α-TNCoPc and β-TNCoPc isomers.
(E) In-situ electrochemical mass spectrometry with β-TNCoPc isomer during the charge reaction.
(F) Long-term cycling with β-TNCoPc isomer at a current density of 20 mA/cm^2.

Figure 4. Post-electrochemical characterization of isomeric electrocatalysts.

(A) XPS spectra of β-TNCoPc composite electrode before (violet) and after (red) long term polarization for 70 hours.
(B) UV-visible spectra before (violet) and after (red) long term polarization for 70 hours.
(C) FT-IR spectra before (violet) and after (red) long term polarization for 70 hours.
(D) Raman spectra before (violet) and after (red) long term polarization for 70 hours.

STAR METHODS

RESOURCE AVAILABILITY

Lead contact

Further information and requests for resources should be directed to and will be fulfilled by the lead contact, Musthafa Ottakam Thotiyl (musthafa@iiserpune.ac.in).

Materials availability

This study did not generate new unique reagents.

Data and code availability

- There is no original code associated with this work.
- Data reported in this paper will be shared by the lead contact upon request.
- Any additional information required to reanalyze the data reported in this paper will be available from the lead contact upon request.

METHOD DETAILS

Electrochemical measurements

The electrochemical experiments were done using the Biologic potentiostat (VMP 300) at 25°C and 1 atm pressure. For the electrochemical measurements, a three-electrode cell (10 ml volume, 2 mm electrode distance) configuration was used with a 3 mm diameter glassy carbon disk as the working electrode, a platinum wire as the counter electrode and an Ag/AgCl/Cl^- (3.5 M KCl) as the reference electrode. All the potentials were finally converted to reversible hydrogen scale (RHE scale) based on the redox potentials for hydrogen redox reactions obtained on a Pt disc working electrode. Electrochemical investigations were performed in 1 M KOH alkaline solution (pH 14) at a rotation rate of 1600 rpm with (CoPc), (α-TNCoPc) isomer and (β-TNCoPc) isomer modified glassy carbon electrodes. The catalyst ink was prepared by dispersing a known amount of catalyst in isopropyl alcohol with 5 wt % Nafion as the binder followed by sonication for 1 hour. The prepared ink was then drop casted on the glassy carbon electrode for preparing the working electrode. The glassy carbon electrode was cleaned each time by polishing with 0.005 µm alumina powder followed by electrochemical cycling in the supporting electrolyte prior to its usage. Before starting the experiment, the solutions were purged with nitrogen gas for about 15 minutes. Rotating Ring Disk Electrode (RRDE) method with GC disk and Au ring electrode was used to calculate number of electrons and H2O2 percentage. Linear sweep voltammetry was carried out on the disc electrode whereas ring was biased at H_2O_2 oxidation potential (1V vs RHE)(Zhou et al., 2016).

The number of electron (n) is calculated using the following equation:

$$n = 4 \times \frac{I_d}{I_d + \frac{I_r}{N_c}}$$

and the % of peroxide (p) produced was calculated with the following equation:

$$p = 2 \times \frac{\frac{I_r}{N_c}}{I_d + \frac{I_r}{N_c}}$$

where I_d, I_r and N_c represents the disk current, ring current and collection efficiency of the RRDE respectively. N_c was found to be 0.37 which was calculated by measuring the ratio of disk current to ring current in equimolar concentrations of potassium ferrocyanide and potassium ferricyanide. Polarization and constant current tests for the battery were performed in a tri-electrode two-compartment flood cell configuration in full cell mode (Scheme S1) at 25°C and 1 atm pressure. The two half-cells were separated by a Nafion-117 membrane. The anodic compartment contained zinc metal dipped in 0.2 M Zn $(OAc)_2$ solution dissolved in 6 M KOH solution (30 mL). Cathodic compartment contained oxygen purged (100 ml/min) 6 M KOH solution (30 mL). The cathodic compartment housed both the ORR catalyst i.e., Pt/C with a catalyst loading of 0.5 mg/cm^2 as well as the OER catalyst i.e., β-TNCoPc, α-TNCoPc and unsubstituted CoPc with a catalyst loading of 2 mg/cm^2 on a carbon paper. The catalyst inks were prepared by dispersing a known amount of the phthalocyanine/CNT (30:70) in iso propyl alcohol with 5 wt % Nafion dispersion as the binder.

Materials characterization

UV-Visible measurements of the molecules were carried out using a Perkin Elmer Lambda 950 instrument. FTIR spectra of the pristine CoPc, α-TNCoPc isomer and β-TNCoPc isomer as well as the molecules anchored on CNT were done using a Bruker Alpha ATR-FTIR spectrometer. Raman spectra were recorded using a Raman microscope (LabRAM HR, Horbia Jobin Yvon). Scanning electron microscopy with energy dispersive X-ray spectrum was carried out with Zeiss Ultraplus-4095 instrument for checking the morphology and elemental analysis. Nuclear magnetic resonance (NMR) spectra of isomeric molecules were recorded with Bruker 400 MHz spectrometer. In-situ electrochemical mass spectrometry was carried out with an HPR-40 R&D (Hiden analytical) Quadruple mass analyzer with a standard QIC inlet. The intensity count is represented as relative pressure with respect to a carrier gas. X-ray photo electron spectroscopy (XPS) measurements were obtained with a ThermoKalpha$^+$ spectrometer using a monochromated Al Kα (1486.6 eV) X-ray source having 72 W power. The spot size of the X-rays was kept at 400 µm. 180^o double focusing hemispherical analyzer with 128 channel detector was used for electron energy analysis. Charge compensation was done with ultra-low energy co-axial electron and Ar+ ion beam and was always switched on during the spectral acquisition and final spectra were cross verified for charge accumulation with C1s standard value at 284.6 eV. The base pressure of the spectrometer was always better than ~$5x10^{-9}$

mbar and ~1x10^{-7} mbar during data acquisition with flood gun on. The survey scan was collected at 200 eV pass energy and individual core-levels at 50 eV.

SUPPLEMENTAL INFORMATION

Document S1. Supplemental experimental procedures, Figures S1–S9, Tables S1–S5 and Scheme S1

REFERENCES

Davidson, D.J., 2019. Exnovating for a renewable energy transition. Nature Energy 4, 254–256. https://doi.org/10.1038/s41560-019-0369-3

Gao, J., Shang, K., Ding, Y., Wen, Z., 2021. Material and configuration design strategies towards flexible and wearable power supply devices: a review. Journal of Materials Chemistry A 9, 8950–8965. https://doi.org/10.1039/d0ta11260g

Ledendecker, M., Krick Calderón, S., Papp, C., Steinrück, H.-P., Antonietti, M., Shalom, M., 2015. The Synthesis of Nanostructured Ni5P4 Films and their Use as a Non-Noble Bifunctional Electrocatalyst for Full Water Splitting. Angewandte Chemie International Edition 54, 12361–12365. https://doi.org/https://doi.org/10.1002/anie.201502438

Chinnam, P.R., Clymer, R.N., Jalil, A.A., Wunder, S.L., Zdilla, M.J., 2015. Bulk-Phase Ion Conduction in Cocrystalline LiCl·N,N-Dimethylformamide: A New Paradigm for Solid Electrolytes Based upon the Pearson Hard-Soft Acid-Base Concept. Chemistry of Materials 27, 5479–5482. https://doi.org/10.1021/acs.chemmater.5b00940

Indra, A., Song, T., Paik, U., 2018. Metal Organic Framework Derived Materials: Progress and Prospects for the Energy Conversion and Storage. Advanced Materials 30, 1–25. https://doi.org/10.1002/adma.201705146

Liberman, I., Shimoni, R., Ifraemov, R., Rozenberg, I., Singh, C., Hod, I., 2020. Active-Site Modulation in an Fe-Porphyrin-Based Metal–Organic Framework through Ligand Axial Coordination: Accelerating Electrocatalysis and Charge-Transport Kinetics. Journal of the American Chemical Society 142, 1933–1940. https://doi.org/10.1021/jacs.9b11355

Zhao, Y., Pei, Z., Lu, X.F., Luan, D., Wang, X., Lou, X.W. (David), 2022. Rationally designed nitrogen-doped carbon macroporous fibers with loading of single cobalt sites for efficient aqueous Zn-CO_2 batteries. Chem Catalysis 2, 1480–1493. https://doi.org/10.1016/j.checat.2022.05.015

Harper, G., Sommerville, R., Kendrick, E., Driscoll, L., Slater, P., Stolkin, R., Walton, A., Christensen, P., Heidrich, O., Lambert, S., Abbott, A., Ryder, K., Gaines, L., Anderson, P., 2019. Recycling lithium-ion batteries from electric vehicles. Nature 575, 75–86. https://doi.org/10.1038/s41586-019-1682-5

Li, W., Zhu, J., Xia, Y., Gorji, M.B., Wierzbicki, T., 2019. Data-Driven Safety Envelope of Lithium-Ion Batteries for Electric Vehicles. Joule 3, 2703–2715. https://doi.org/10.1016/j.joule.2019.07.026

Zhang, J., Quast, T., He, W., Dieckhöfer, S., Junqueira, J.R.C., Öhl, D., Wilde, P., Jambrec, D., Chen, Y., Schuhmann, W., 2022. In-situ Carbon Corrosion and Cu Leaching as a Strategy for Boosting Oxygen Evolution Reaction in multi-metal Electrocatalysts. Advanced Materials 2109108. https://doi.org/10.1002/adma.202109108

Tabassum, H., Mahmood, A., Zhu, B., Liang, Z., Zhong, R., Guo, S., Zou, R., 2019. Recent advances in confining metal-based nanoparticles into carbon nanotubes for electrochemical energy conversion and storage devices. Energy and Environmental Science 12, 2924–2956. https://doi.org/10.1039/c9ee00315k

Bruce, P.G., Freunberger, S.A., Hardwick, L.J., Tarascon, J.M., 2012. LigO2 and LigS batteries with high energy storage. Nature Materials 11, 19–29. https://doi.org/10.1038/nmat3191

Lee, J.S., Kim, S.T., Cao, R., Choi, N.S., Liu, M., Lee, K.T., Cho, J., 2011. Metal-air batteries with high energy density: Li-air versus Zn-air. Advanced Energy Materials 1, 34–50. https://doi.org/10.1002/aenm.201000010

Jung, J. Il, Risch, M., Park, S., Kim, M.G., Nam, G., Jeong, H.Y., Shao-Horn, Y., Cho, J., 2016. Optimizing nanoparticle perovskite for bifunctional oxygen electrocatalysis. Energy and Environmental Science 9, 176–183. https://doi.org/10.1039/c5ee03124a

Li, R.Q., Liu, Q., Zhou, Y., Lu, M., Hou, J., Qu, K., Zhu, Y., Fontaine, O., 2021. 3D self-supported porous vanadium-doped nickel nitride nanosheet arrays as efficient bifunctional electrocatalysts for urea electrolysis. Journal of Materials Chemistry A 9, 4159–4166. https://doi.org/10.1039/d0ta09473k

Liu, X., Yuan, Y., Liu, J., Liu, B., Chen, X., Ding, J., Han, X., Deng, Y., Zhong, C., Hu, W., 2019. Utilizing solar energy to improve the oxygen evolution reaction kinetics in zinc–air battery. Nature Communications 10. https://doi.org/10.1038/s41467-019-12627-2

Guo, X., Zheng, T., Ji, G., Hu, N., Xu, C., Zhang, Y., 2018. Core/shell design of efficient electrocatalysts based on NiCo2O4 nanowires and NiMn LDH nanosheets for rechargeable zinc-air batteries. Journal of Materials Chemistry A 6, 10243–10252. https://doi.org/10.1039/c8ta02608d

Liu, X., Park, M., Kim, M.G., Gupta, S., Wang, X., Wu, G., Cho, J., 2016. High-performance non-spinel cobalt–manganese mixed oxide-based bifunctional electrocatalysts for rechargeable zinc–air batteries. Nano Energy 20, 315–325. https://doi.org/https://doi.org/10.1016/j.nanoen.2015.11.030

Fu, J., Cano, Z.P., Park, M.G., Yu, A., Fowler, M., Chen, Z., 2017. Electrically Rechargeable Zinc–Air Batteries: Progress, Challenges, and Perspectives. Advanced Materials 29. https://doi.org/10.1002/adma.201604685

Peng, Y., Zhang, F., Zhang, Y., Luo, X., Chen, L., Shi, Y., 2022. ZnS modified N, S dual-doped interconnected porous carbon derived from dye sludge waste as high-efficient ORR/OER catalyst for

rechargeable zinc-air battery. Journal of Colloid and Interface Science 616, 659–667. https://doi.org/https://doi.org/10.1016/j.jcis.2022.02.102

Özen, Ü.E., Doğan, E., Özer, M., Bekaroğlu, Ö., Özkaya, A.R., 2016. Communication—High-Performance and Non-Precious Bifunctional Oxygen Electrocatalysis with Binuclear Ball-Type Phthalocyanine Based Complexes for Zinc-Air Batteries. Journal of The Electrochemical Society 163, A2001–A2003. https://doi.org/10.1149/2.0941609jes

Xu, H., Ci, S., Ding, Y., Wang, G., Wen, Z., 2019. Recent advances in precious metal-free bifunctional catalysts for electrochemical conversion systems. Journal of Materials Chemistry A 7, 8006–8029. https://doi.org/10.1039/c9ta00833k

Li, Q., Han, L., Luo, Q., Liu, X., Yi, J., 2022. Towards Understanding the Corrosion Behavior of Zinc-Metal Anode in Aqueous Systems: From Fundamentals to Strategies. Batteries & Supercaps 5, e202100417. https://doi.org/https://doi.org/10.1002/batt.202100417

Lee, D.U., Choi, J.Y., Feng, K., Park, H.W., Chen, Z., 2014. Advanced extremely durable 3D bifunctional air electrodes for rechargeable zinc-air batteries. Advanced Energy Materials 4, 1–5. https://doi.org/10.1002/aenm.201301389

Cherevko, S., Geiger, S., Kasian, O., Kulyk, N., Grote, J.P., Savan, A., Shrestha, B.R., Merzlikin, S., Breitbach, B., Ludwig, A., Mayrhofer, K.J.J., 2016. Oxygen and hydrogen evolution reactions on Ru, RuO2, Ir, and IrO2 thin film electrodes in acidic and alkaline electrolytes: A comparative study on activity and stability. Catalysis Today 262, 170–180. https://doi.org/10.1016/j.cattod.2015.08.014

Ghareghashi, A., Mohebbi, A., 2020. Anode Materials for Zinc-Air Batteries. Zinc Batteries 103–130. https://doi.org/10.1002/9781119662433.ch8

Bhowmick, S., Dhankhar, A., Sahu, T.K., Jena, R., Gogoi, D., Peela, N.R., Ardo, S., Qureshi, M., 2020. Low Overpotential and Stable Electrocatalytic Oxygen Evolution Reaction Utilizing Doped Perovskite Oxide, La0.7Sr0.3MnO3, Modified by Cobalt Phosphate. ACS Applied Energy Materials 3, 1279–1285. https://doi.org/10.1021/acsaem.9b02167

Anju, V.G., Manjunatha, R., Austeria, P.M., Sampath, S., 2016. Primary and rechargeable zinc-air batteries using ceramic and highly stable TiCN as an oxygen reduction reaction electrocatalyst. Journal of Materials Chemistry A 4, 5258–5264. https://doi.org/10.1039/c6ta00377j

Sobbi, A.K., Wöhrie, D., Schlettwein, D., 1993. Photochemical stability of various porphyrins in solution and as thin film electrodes. Journal of the Chemical Society, Perkin Transactions 2 481–488. https://doi.org/10.1039/p2993000481

Bottari, G., Torre, G. De, Guldi, D.M. and T.T., 2010. Covalent and Noncovalent Phthalocyanine-Carbon Nanostructure Systems Solar cell. Chem. Rev. 110, 6768–6816.

Complexes, N.M., 2007. N4-macrocyclic metal complexes, Choice Reviews Online. https://doi.org/10.5860/choice.44-3301

Sorokin, A.B., 2013. Phthalocyanine Metal Complexes in Catalysis BT - Chemical Reviews. Chemical Reviews 113, 8152–8191.

Kottaichamy, A.R., Begum, S., Nazrulla, M.A., Dargily, N.C., Devendrachari, M.C., Manzoor Bhat, Z., Thimmappa, R., Makri Nimbegondi Kotresh, H., Vinod, C.P., Thotiyl, M.O., 2020. Unprecedented Isomerism-Activity Relation in Molecular Electrocatalysis. Journal of Physical Chemistry Letters 11, 263–271. https://doi.org/10.1021/acs.jpclett.9b02689

Cong, F. Di, Ning, B., Yu, H.F., Cui, X.J., Chen, B., Cao, S.G., Ma, C.Y., 2005. The control of phthalocyanine properties through nitro-group electronic effect. Spectrochimica Acta - Part A: Molecular and Biomolecular Spectroscopy 62, 394–397. https://doi.org/10.1016/j.saa.2005.01.006

Fu, Y., Xu, D., Wang, Y., Li, X., Chen, Z., Li, K., Li, Z., Zheng, L., Zuo, X., 2020. Single Atoms Anchored on Cobalt-Based Catalysts Derived from Hydrogels Containing Phthalocyanine toward the Oxygen Reduction Reaction. ACS Sustainable Chemistry & Engineering 8, 8338–8347. https://doi.org/10.1021/acssuschemeng.0c02158

Li, C., Huang, T., Huang, Z., Sun, J., Zong, C., Yang, J., Deng, W., Dai, F., 2019. A sulfonated cobalt phthalocyanine/carbon nanotube hybrid as a bifunctional oxygen electrocatalyst. Dalton Transactions 48, 17258–17265. https://doi.org/10.1039/C9DT03360B

Li, R., Zhang, X., Zhu, P., Ng, D.K.P., Kobayashi, N., Jiang, J., 2006. Electron-donating or -withdrawing nature of substituents revealed by the electrochemistry of metal-free phthalocyanines. Inorganic Chemistry 45, 2327–2334. https://doi.org/10.1021/ic051931k

Kobayashi, N., Miwa, H., Nemykin, V.N., 2002. Adjacent versus opposite type di-aromatic ring-fused phthalocyanine derivatives: Synthesis, spectroscopy, electrochemistry, and molecular orbital calculations. Journal of the American Chemical Society 124, 8007–8020. https://doi.org/10.1021/ja0123812

Panwar, V., Kumar, P., Ray, S.S., Jain, S.L., 2015. Organic inorganic hybrid cobalt phthalocyanine/polyaniline as efficient catalyst for aerobic oxidation of alcohols in liquid phase. Tetrahedron Letters 56, 3948–3953. https://doi.org/10.1016/j.tetlet.2015.05.003

Topuz, B.B., Gündüz, G., Mavis, B., Çolak, Ü., 2013. Synthesis and characterization of copper phthalocyanine and tetracarboxamide copper phthalocyanine deposited mica-titania pigments. Dyes and Pigments 96, 31–37. https://doi.org/10.1016/j.dyepig.2012.06.010

Zhu, L., Jing, X., Song, L., Liu, B., Zhou, Y., Xiang, Y., Xia, D., 2014. Solid-phase synthesis and catalytic sweetening performance of sulfonated cobalt phthalocyanine from sulfonated phthalic anhydride mixture. New Journal of Chemistry 38, 663–668. https://doi.org/10.1039/c3nj01063e

Georgescu, R., Boscornea, C., Calinescu, I., State, R., 2015. Raman, IR and UV-Vis spectroscopic investigations of some substituted phthalocyanines. Revista de Chimie 66, 1554–1557.

Zhang, M., Gorski, W., 2005. Electrochemical sensing platform based on the carbon nanotubes/redox mediators-biopolymer system. Journal of the American Chemical Society 127, 2058–2059. https://doi.org/10.1021/ja044764g

Abbaspour, A., Mirahmadi, E., 2013. Electrocatalytic activity of iron and nickel phthalocyanines supported on multi-walled carbon nanotubes towards oxygen evolution reaction. Electrochimica Acta 105, 92–98. https://doi.org/10.1016/j.electacta.2013.04.143

Chidembo, A.T., Ozoemena, K.I., Agboola, B.O., Gupta, V., Wildgoose, G.G., Compton, R.G., 2010. Nickel(ii) tetra-aminophthalocyanine modified MWCNTs as potential nanocomposite materials for the development of supercapacitors. Energy and Environmental Science 3, 228–236. https://doi.org/10.1039/b915920g

Zhu, J., Li, Y., Chen, Y., Wang, J., Zhang, B., Zhang, J., Blau, W.J., 2011. Graphene oxide covalently functionalized with zinc phthalocyanine for broadband optical limiting. Carbon 49, 1900–1905. https://doi.org/10.1016/j.carbon.2011.01.014

Zhang, Xing, Wu, Z., Zhang, Xiao, Li, L., Li, Y., Xu, H., Li, X., Yu, X., Zhang, Z., Liang, Y., Wang, H., 2017. Highly selective and active CO2 reduction electrocatalysts based on cobalt phthalocyanine/carbon nanotube hybrid structures. Nature Communications 8, 1–8. https://doi.org/10.1038/ncomms14675

Shi, X., Back, S., Gill, T.M., Siahrostami, S., Zheng, X., 2021. Electrochemical Synthesis of H2O2 by Two-Electron Water Oxidation Reaction. Chem 7, 38–63. https://doi.org/10.1016/j.chempr.2020.09.013

Xia, C., Back, S., Ringe, S., Jiang, K., Chen, F., Sun, X., Siahrostami, S., Chan, K., Wang, H., 2020. Confined local oxygen gas promotes electrochemical water oxidation to hydrogen peroxide. Nature Catalysis 3, 125–134. https://doi.org/10.1038/s41929-019-0402-8

Gill, T.M., Vallez, L., Zheng, X., 2021. The Role of Bicarbonate-Based Electrolytes in H2O2Production through Two-Electron Water Oxidation. ACS Energy Letters 6, 2854–2862. https://doi.org/10.1021/acsenergylett.1c01264

Malali, S., Manzoor, Z., Ottakam, M., 2020. Journal of Colloid and Interface Science A zinc-quinone battery for paired hydrogen peroxide electrosynthesis. Journal of Colloid and Interface Science 559, 324–330. https://doi.org/10.1016/j.jcis.2019.10.031

Zhang, Q., Zhou, M., Ren, G., Li, Yawei, Li, Yanchun, Du, X., 2020. Highly efficient electrosynthesis of hydrogen peroxide on a superhydrophobic three-phase interface by natural air diffusion. Nature Communications 11, 1731. https://doi.org/10.1038/s41467-020-15597-y

Wu, K.-H., Wang, D., Lu, X., Zhang, X., Xie, Z., Liu, Y., Su, B.-J., Chen, J.-M., Su, D.-S., Qi, W., Guo, S., 2020. Highly Selective Hydrogen Peroxide Electrosynthesis on Carbon: In Situ Interface Engineering with Surfactants. Chem 6, 1443–1458. https://doi.org/https://doi.org/10.1016/j.chempr.2020.04.002

Gu, W., Hu, L., Hong, W., Jia, X., Li, J., Wang, E., 2016. Noble-metal-free Co3S4–S/G porous hybrids as an efficient electrocatalyst for oxygen reduction reaction. Chemical Science 7, 4167–4173. https://doi.org/10.1039/C6SC00357E

Rodríguez-fernández, J., Sun, Z., Zhang, L., Tan, T., Curto, A., Lauritsen, J. V, 2019. Structural and electronic properties of Fe dopants in cobalt oxide nanoislands on Structural and electronic properties of Fe dopants in cobalt oxide nanoislands on Au (111) 041731. https://doi.org/10.1063/1.5052336

Thapa, S., Paudel, R., Blanchet, M.D., Gemperline, P.T., Comes, R.B., 2021. Probing surfaces and interfaces in complex oxide films via in situ X-ray photoelectron spectroscopy. Journal of Materials Research 36, 26–51. https://doi.org/10.1557/s43578-020-00070-9

Cao, R., Thapa, R., Kim, H., Xu, X., Kim, M.G., Li, Q., Park, N., Liu, M., Cho, J., 2013. Promotion of oxygen reduction by a bio-inspired tethered iron phthalocyanine carbon nanotube-based catalyst. Nature Communications 4, 1–7. https://doi.org/10.1038/ncomms3076

Tran, T.N.T., Clark, M.P., Xiong, M., Chung, H.J., Ivey, D.G., 2020. A tri-electrode configuration for zinc-air batteries using gel polymer electrolytes. Electrochimica Acta 357, 136865. https://doi.org/10.1016/j.electacta.2020.136865

Hong, W., Li, H., Wang, B., 2016. A horizontal three-electrode structure for zinc-air batteries with long-term cycle life and high performance. International Journal of Electrochemical Science 11, 3843–3851. https://doi.org/10.20964/110384

Yu, Q., Xu, J., Wu, C., Zhang, J., Guan, L., 2016. MnO2 Nanofilms on Nitrogen-Doped Hollow Graphene Spheres as a High-Performance Electrocatalyst for Oxygen Reduction Reaction. ACS Applied Materials and Interfaces 8, 35264–35269. https://doi.org/10.1021/acsami.6b11870

Yang, T.B., Zhou, K.Y., Chen, G.Y., Zhang, W.X., Liang, J.C., 2017. CoSb3 alloy nanoparticles wrapped with N-doped carbon layers as a highly active bifunctional electrocatalyst for zinc-air batteries. RSC Advances

7, 33012–33019. https://doi.org/10.1039/c7ra04789d

Li, Y., Qiu, W., Qin, F., Fang, H., Hadjiev, V.G., Litvinov, D., Bao, J., 2016. Identification of Cobalt Oxides with Raman Scattering and Fourier Transform Infrared Spectroscopy. Journal of Physical Chemistry C 120, 4511–4516. https://doi.org/10.1021/acs.jpcc.5b11185

Tang, C.W., Wang, C. Bin, Chien, S.H., 2008. Characterization of cobalt oxides studied by FT-IR, Raman, TPR and TG-MS. Thermochimica Acta 473, 68–73. https://doi.org/10.1016/j.tca.2008.04.015

Barakat, N.A.M., Khil, M.S., Sheikh, F.A., Kim, H.Y., 2008. Synthesis and optical properties of two cobalt oxides (CoO and Co 3O4) nanoflbers produced by electrospinning process. Journal of Physical Chemistry C 112, 12225–12233. https://doi.org/10.1021/jp8027353

Brillas, E., Alcaide, F., Cabot, P.-L., 2002. A small-scale flow alkaline fuel cell for on-site production of hydrogen peroxide. Electrochimica Acta 48, 331–340. https://doi.org/https://doi.org/10.1016/S0013-4686(02)00665-5

Li, W., Bonakdarpour, A., Gyenge, E., Wilkinson, D.P., 2013. Drinking Water Purification by Electrosynthesis of Hydrogen Peroxide in a Power-Producing PEM Fuel Cell. ChemSusChem 6, 2137–2143. https://doi.org/https://doi.org/10.1002/cssc.201300225

Zhou, R., Zheng, Y., Jaroniec, M., Qiao, S.Z., 2016. Determination of the Electron Transfer Number for the Oxygen Reduction Reaction: From Theory to Experiment. ACS Catalysis 6, 4720–4728. https://doi.org/10.1021/acscatal.6b01581

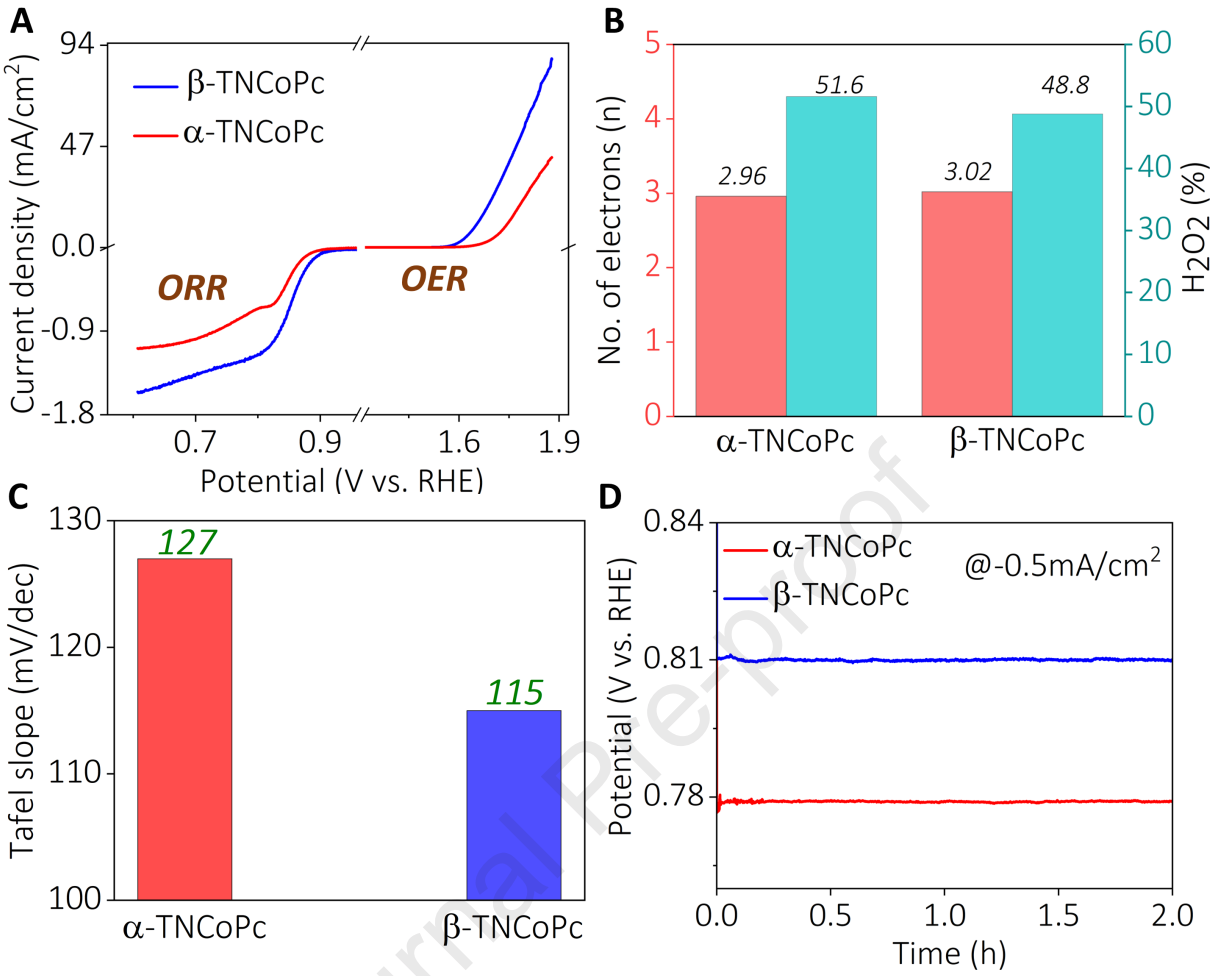

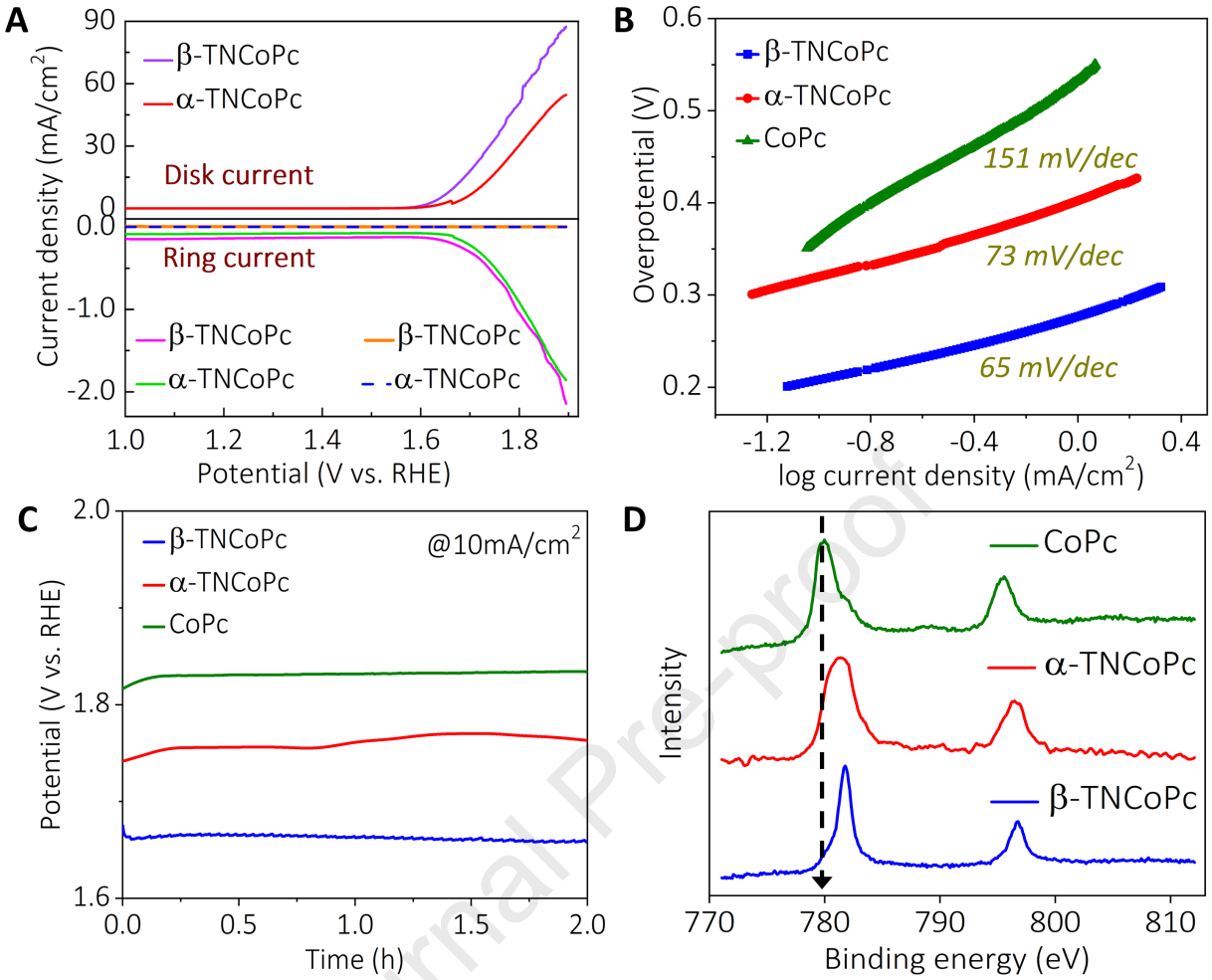

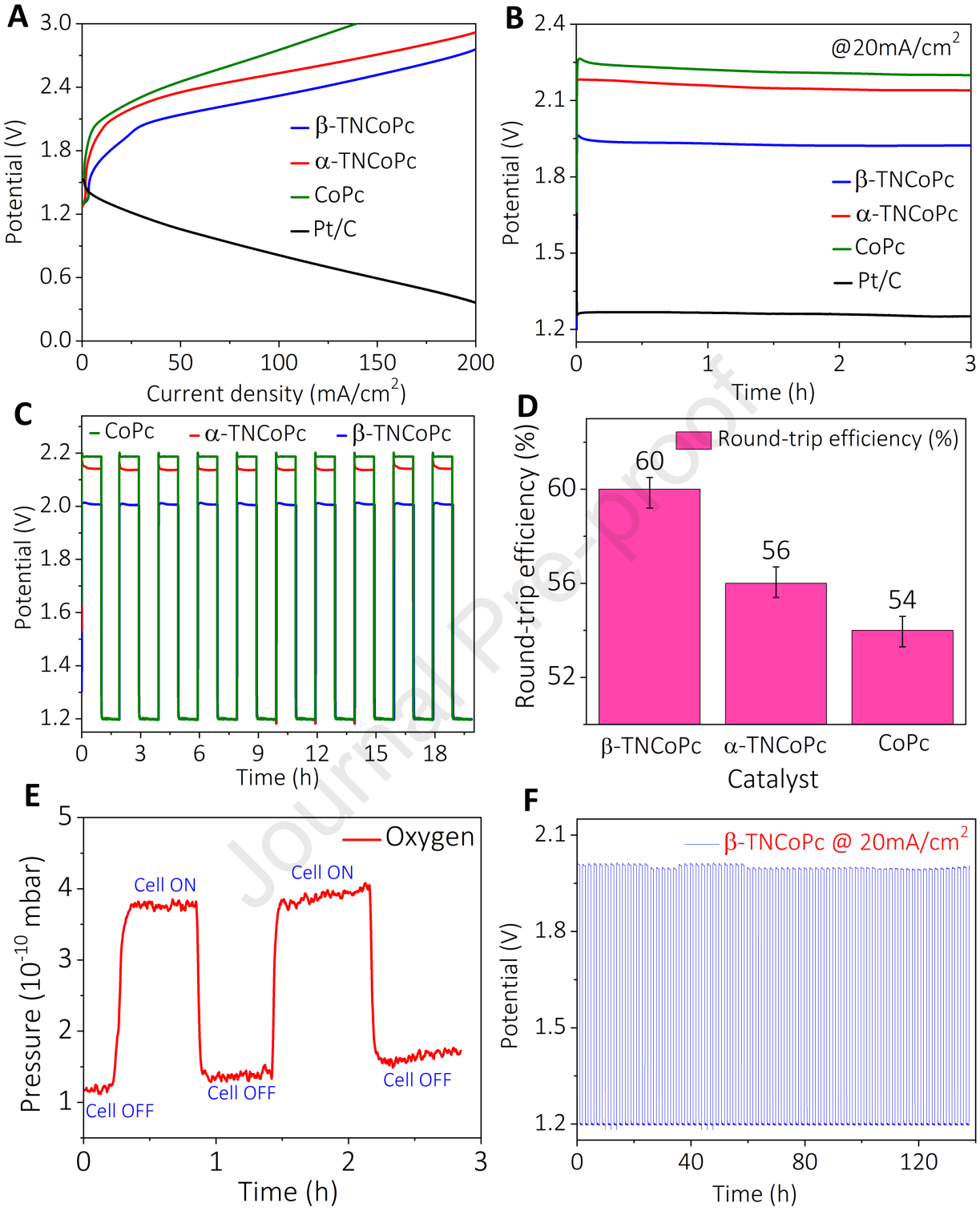

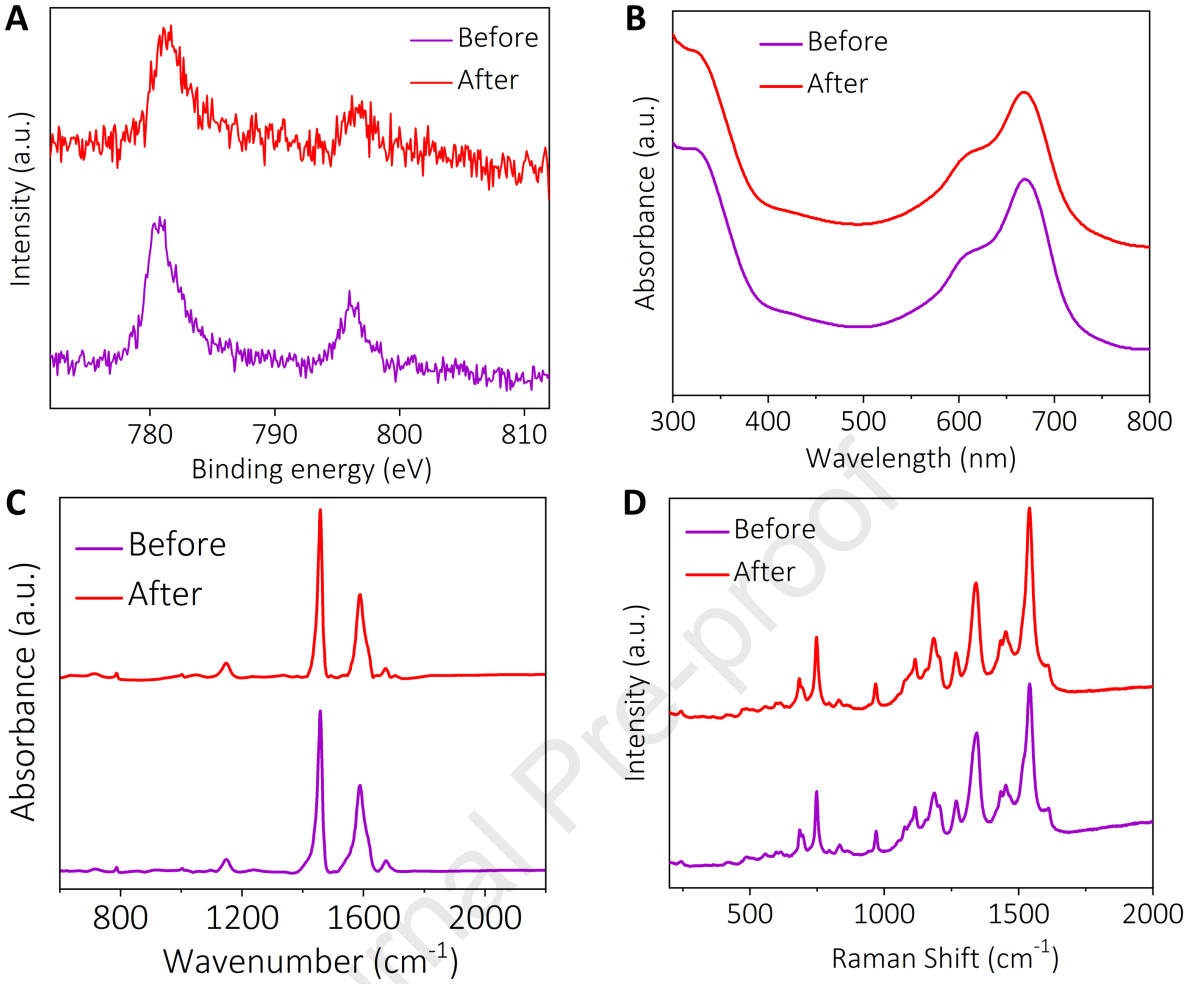

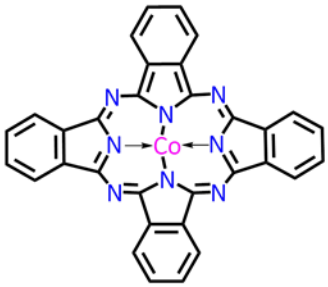

CoPc

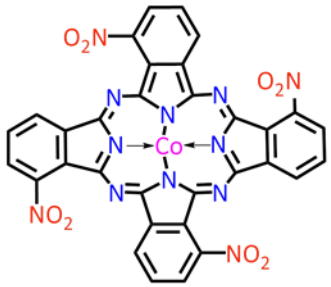

α-TNCoPc

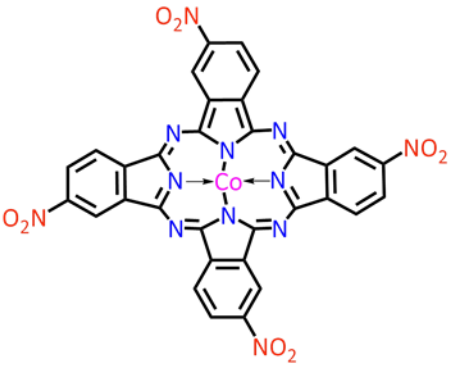

β-TNCoPc

- Ligand isomerism tunes the activity of the catalytic centre.
- Repulsive non-covalent interactions are responsible for the catalytic activation.
- Ligand isomerism can improve the round-trip efficiency of a Zn-air battery.

KEY RESOURCES TABLE

REAGENT or RESOURCE	SOURCE	IDENTIFIER
Other		
Ammonium molybdate, 99.99% (metal basis)	Alfa Aesar	https://www.alfa.com/en/catalog/043206/
N, N-Dimethylformamide, 99%	Alfa Aesar	https://www.alfa.com/en/catalog/A13547/
Hydrogen peroxide, 35%	Alfa Aesar	https://www.alfa.com/en/catalog/L14000/
3-Nitrophthalimide, 98%	Alfa Aesar	https://www.alfa.com/en/catalog/A15291/
4-Nitrophthalimide, 98%	Alfa Aesar	https://www.alfa.com/en/catalog/A12040/
Phthalimide, 99%	Alfa Aesar	https://www.alfa.com/en/catalog/A12584/
Cobalt (II) chloride hexahydrate, 98%	Alfa Aesar	https://www.alfa.com/en/catalog/A16346/
Zinc chloride hydrate, 99.99% (metal basis)	Alfa Aesar	https://www.alfa.com/en/catalog/041247/
Urea, 99.0-100.5%	Alfa Aesar	https://www.alfa.com/en/catalog/036428/
Ammonium chloride, 98+%	Alfa Aesar	https://www.alfa.com/en/catalog/A15000/
Nitrobenzene, 99%	Alfa Aesar	https://www.alfa.com/en/catalog/A10585/
2-Propanol, 99.5%	Alfa Aesar	https://www.alfa.com/en/catalog/036644/
Ethanol, 94-96%	Alfa Aesar	https://www.alfa.com/en/catalog/033361/
Methanol, 99%	Alfa Aesar	https://www.alfa.com/en/catalog/L13255/
Toluene, 99%	Alfa Aesar	https://www.alfa.com/en/catalog/L10967/
n-Hexane, 99%	Alfa Aesar	https://www.alfa.com/en/catalog/L09938/
Potassium hydroxide, pellets, 85%	Alfa Aesar	https://www.alfa.com/en/catalog/A18854/
Potassium hexacyanoferrate (III), 98+%	Alfa Aesar	https://www.alfa.com/en/catalog/A16946/
Potassium hexacyanoferrate (II) trihydrate, 98+%	Alfa Aesar	https://www.alfa.com/en/catalog/A15736/
Zinc acetate dihydrate, 97+%	Alfa Aesar	https://www.alfa.com/en/catalog/A12909/
Hydrochloric acid, 37%	Sigma Aldrich	SKU: 258148-100ML
Perfluorinated resin solution containing Nafion	Sigma Aldrich	SKU: 274704-100ML
Carbon nanotube, multi-walled	Sigma Aldrich	SKU: 698849-1G